Journal of Colloid and Interface Science 683 (2025) 620–630

Contents lists available at ScienceDirect

Journal of Colloid And Interface Science

journal homepage: www.elsevier.com/locate/jcis

Regular Article

Supramolecular dextran/polyamine phosphate nanocapsules with smart responsiveness for encapsulation of therapeutics

Aharon Steffè [a,1,2], Francesca Milano [a,1], Santiago Giménez Reyes [b,c], Francesca Buco [a], Riccardo Leonetti [d], Yessica Roque-Diaz [d], Sofia Zuffi [b,e], Paolo Di Gianvincenzo [b], Angela Roberta Cortese [a], Hernan Ritacco [c], Patrizia Andreozzi [a], Maria Grazia Ortore [d], Sergio E. Moya [b,*], Marco Marradi [a,*]

[a] Department of Chemistry 'Ugo Schiff', University of Florence, via della Lastruccia 3-13, 50019 Sesto Fiorentino (FI), Italy
[b] Soft Matter Nanotechnology Group, CIC biomaGUNE, Basque Research and Technology Alliance (BRTA), Paseo Miramón 182, 20014 Donostia-San Sebastián, Guipúzcoa, Spain
[c] Instituto de Física del Sur (IFISUR), Departamento de Física, Universidad Nacional del Sur (UNS), CONICET, Av. Alem 1253, Bahía Blanca 8000, Argentina
[d] Department of Life and Environmental Sciences, Marche Polytechnic University, via Brecce Bianche, 60131 Ancona, Italy
[e] Molecular Oncology Laboratory, IIS BioGipuzkoa, P° Dr. Beguiristain s/n, 20014 San Sebastián, Gipuzkoa, Spain

HIGHLIGHTS

- Dextran (DEX)-polyallylamine (PAH) assembles in phosphate buffer with different morphology depending on DEX loading.
- PAH modified with one DEX chain per polyamine form glyconanocapsules with sizes around 100 nm.
- PAH:DEX glyconanocapsules assemble and disassemble in response to external pH.
- pH sensibility of glyconanocapsules can be used for protein entrapment and release.

GRAPHICAL ABSTRACT

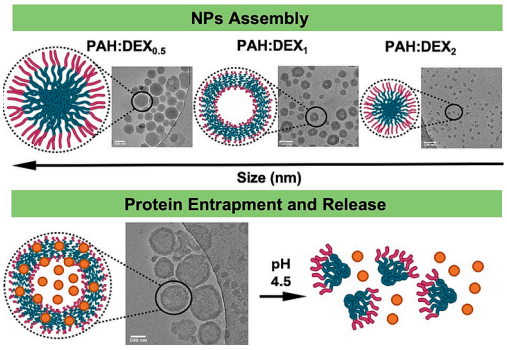

ARTICLE INFO

Keywords:
Smart glyconanomaterials
Polyamine phosphate nanoparticles
Nanocapsules

ABSTRACT

The polyallylamine hydrochloride (PAH) polymer is here functionalized with branched and biocompatible polysaccharide dextran (DEX) molecules. Covalent conjugation of DEX to PAH has been achieved through a straightforward reductive amination approach, allowing for a controlled number of DEX chains per PAH polymer

Abbreviations: BCA, Bicinchoninic acid; BSA, Bovine serum albumin; CD, Circular dichroism; cryo-EM, Cryogenic electron microscopy; DEX, Dextran; DLS, Dynamic light scattering; FCS, Fluorescence correlation spectroscopy; NMR, Nuclear Magnetic Resonance; NCs, Nanocapsules; NPs, Nanoparticles; OA, Oleic acid; PAH, Poly(allylamine hydrochloride) salt; PANs, Phosphate polyamine nanoparticles; PB, Phosphate buffer; PBS, Phosphate buffer saline; PEG, Polyethylene glycol; RBITC, Rhodamine B isothiocyanate; r.t., Room temperature; SAXS, Small-angle X-ray scattering; UV–Vis, Ultraviolet–visible spectroscopy.

* Corresponding authors.
E-mail addresses: smoya@cicbiomagune.es (S.E. Moya), marco.marradi@unifi.it (M. Marradi).
[1] These authors contributed equally.
[2] Current address: Dipartimento di Scienze Chimiche e Farmaceutiche (DSCF), Università degli Studi di Trieste, Via L. Giorgieri, 1, 34127 Trieste, Italy.

https://doi.org/10.1016/j.jcis.2024.12.074
Received 6 September 2024; Received in revised form 9 December 2024; Accepted 10 December 2024
Available online 12 December 2024

pH responsiveness
Fluorescence correlation spectroscopy (FCS)
Cryogenic transmission electron microscopy (cryo-EM)
Small angle X-ray scattering (SAXS)

(PAH:DEX_n, n = 0.1, 0.5, 1, 2, 5, 10). When exposed to phosphate buffer, PAH:DEX_n polymers form supramolecular assemblies. Physico chemical characteristics and pH responsiveness of the assemblies are correlated with the number of dextran chains per PAH molecule. Nanocapsules (NCs) are formed when PAH:DEX ratio is 1. Capsule formation is explained by the branched nature of DEX and steric consideration ruling the organization of polyamine chains in phosphate buffer. NCs and glyconanoparticles formed with $n < 1$ are responsive to pH changes, being disassembled at endosomal $pH < 6$ and reassembled when $6 < pH < 9$. Dynamic light Scattering (DLS), ζ-potential measurements, cryo-Electron Microscopy and Small Angle X-ray Scattering (SAXS) provided key information about their structure, morphology, size, polydispersity, surface charge, and stability over time. Protein entrapment into the NCs and pH-dependent release is demonstrated with bovine serum albumin (BSA) as model protein by diffusion measurements in fluorescence correlation spectroscopy (FCS), following changes in BSA conformation before and after triggering NC disassembly by circular dichroism (CD), and comparing NCs SAXS fingerprints with and without BSA. Our results show novel assemblies based on polyamine phosphate interactions with capacity of loading large molecules through the formation of capsules, which may find applications in the endosomal delivery of therapeutic proteins and enzymes.

1. Introduction

Loading therapeutics into suitable nanocarriers is of outmost importance to address the challenge of stimuli-responsive and targeted drug delivery [1,2]. pH-responsive nanoparticles have recently called the attention because of their high therapeutic potential for targeted delivery due to their capacity to release encapsulated therapeutics in response to pH changes [3]. Differences in pH values can be found in organs and tissues, as well as between cell interior and outside environment, and/or as a consequence of pathological states. This offers many possibilities for triggering pH-mediated selective delivery [4]. Bloodstream pH is 7.4, but it reduces to pH ≈ 6.5 intracellularly, in the early endosomal compartment, further decreasing to values below pH 5 in the lysosomal compartment [5]. Endosomes become more acidic inside cancer cells and tumor microenvironment is usually more acidic than healthy tissue (pH ≈ 6.4–6.8). pH-responsive NPs can be hence successfully designed to disassembly and/or release their cargo when exposed to these pH stimuli. Supramolecular phosphate polyamine nanoparticles (PANs), formed by electrostatic and hydrogen bonding interactions between phosphate ions and primary amines from the poly (allylamine) hydrochloride (PAH) polymer [6], are an interesting system for intracellular pH stimulated delivery [7–10]. PANs dynamically respond to changes in pH: (i) they are stable at pHs between 6 and 9, (ii) completely disassemble outside this pH range, (iii) reversibly reassemble when they return to the range of pH of stability. This reversibility is indefinitely preserved and makes PANs particularly suitable for cellular and endosomal delivery [7]. Stability at physiological pH 7.4 – the pH of blood – suggests that these nanoparticles will circulate into the bloodstream without disassembling. Instead, when they enter inside cells, the pH of endosomes – around 5.5 – will lead to the protonation of the phosphate groups resulting in the disassembly of the nanoparticles, thus triggering the release of encapsulated cargo [8,11–13]. We have shown that PANs can deliver silencing RNA (siRNA) with good transfection efficiency [14,15]. The positive charges of the polyamine permit the complexation with the phosphate backbone of nucleic acids, supporting polyplex nanoparticle formation and resulting in the same pH responsiveness as those prepared with phosphate buffer (PB). However, polyamines have a drawback: positive charges can induce cytotoxicity, limiting transfection over certain concentrations [16,17]. To enhance their therapeutic window, polyethylene glycol (PEG) and oleic acid (OA) have been used for PAH modification. Oleic acid chemical modification lowered the positive charges of the PAH and resulted in a spontaneous self-assembly of the modified PAH through the hydrophobic chains of OA [18]. Although PAH:OA nanoparticles showed decreased cytotoxicity and an improved *in vitro* transfection efficacy, OA does not fully screen surface charges. Functionalization with PEG is another strategy, which has been widely investigated in several nanomedicines. For instance, PEGylation has been used to increase solubility and reduce cytotoxicity of polyethylenimine (PEI)-DNA complexes without affecting their transfection efficiency [19]. PEG grafting onto polycations has thus proved to be critical to avoid aggregation of complexes, reduce the interaction with serum proteins, and thus boost transgene expression. To further reduce cytotoxicity, some of us modified PAH with PEG chains varying the number of PEG chains per PAH molecule [10,20]. As the number of PEG chains increases per PAH molecule, the resulting core (PAH)/shell (PEG) nanoparticles reduce their size and display practically no surface charge. While PAH:PEG PANs show reduced *in vitro* toxicity through the screening of positive charges, they do not respond to pH changes as compared to PANs prepared with unmodified PAH. This pH stability is likely due to the packing of PEG chains, which is thermodynamically favored. As for PEG, polysaccharides such as dextran (DEX) have been exploited to improve the performance of polyamines. For instance, some studies have demonstrated that DEX plays an essential role in mitigating the high PEI cytotoxicity, improving the stability of polyplexes in presence of serum proteins, and enhancing cellular entry and maintaining transfection efficacy, both *in vitro* [21,22] and *in vivo* [23].

In this work, PAH has been modified with dextran (DEX), a non-charged water-soluble polysaccharide with a characteristic branched structure. Among natural polymers, polysaccharides can be considered as natural analogues of PEG, but with higher biocompatibility [24,25]. Indeed, DEX has been used in several biomedical applications due to aqueous solubility, biocompatibility, biodegradability, wide availability, ease of modification, and non-fouling properties [26–28]. Due to its branched nature, DEX has a larger volume than a PEG of the same molecular weight limiting dense packing arrangements. These characteristics should allow to explore a different organization of DEX chains as compared to the PEG coating. DEX provides biological recognition properties that could also be used for targeted delivery and cell penetration avoiding the need of positive charges for polyplex translocation, too. In this work, DEX has been covalently conjugated to PAH at different molar ratios (PAH:DEX_n, n = 0.1, 0.5, 1, 2, 5, 10), and self-assembled into PANs at different concentrations of PB. PAH:DEX_n PANs display a rich and complex self-assembly behavior, unique among other PAH functionalizations studied. According to the n value, different nanoassemblies are obtained. Interestingly, at PAH:DEX ratio of 1, nanosized core–shell capsules (NCs) are mainly obtained. Instead, at lower or higher n, nanoparticles are formed. When $n \geq 5$ single chain NPs and random coils are obtained. The glycoNCs are responsive systems and can disassemble at endosomal pH values. As a proof of concept, the pH-mediated entrapment in the glycoNCs of bovine serum albumin (BSA) as model protein has been conducted. In this way, we demonstrate that the glycoNCs are interesting nanoscale carriers with supramolecular organization and smart pH responsiveness, which could be exploited for intracellular delivery of therapeutics.

2. Experimental Section

2.1. Materials

Poly(allylamine hydrochloride) salt, 99 % (average M_w 17.5 kDa), dextran (average M_w 6 kDa), sodium cyanoborohydride, 97.9 % ($NaCNBH_3$), Rhodamine B isothiocyanate (RBITC), Bovine Serum Albumin protein, 99 % (BSA), sodium chloride (NaCl) and BCA protein assay kit were purchased from Sigma-Aldrich and used as received. Dialysis was performed using SnakeSkin® Pleated Dialysis Tubing 3500 MWCO purchased from Thermo Fisher or Dialysis Tubing Cellulose Membrane 14,000 MWCO purchased from Sigma-Aldrich.

2.2. General procedure for the preparation of PAH:DEX_n (n = 0.1, 0.5, 1, 2, 5, 10) polymers

DEX and $NaCNBH_3$ were added to a 1.8 mM solution of PAH in borate buffer (0.03 M, pH 8.4). The reaction mixture was kept under magnetic stirring at r.t. and, after 72 h, was loaded into dialysis tubing (cellulose membrane, 14,000 MWCO) which were placed in a 2 L beaker of deionized water. The content of the beaker was gently stirred, recharging with fresh distilled water every 3–4 h over the course of 72 h. Finally, the product was lyophilized and stored at 4 °C. The PAH:DEX_n polymers were analysed by ^{1}H NMR and IR spectroscopy. The assignment of the polymers signals was performed on the basis of the ^{1}H NMR characterization reported in literature for DEX [29] and PAH [10]. ^{1}H NMR spectra are reported in Fig. S1. The specific syntheses of PAH:DEX_n (n = 0.1, 0.5, 1, 2, 5, 10) polymers are reported in SI.

2.3. General procedure for the preparation of fluorescent PAH:RBITC:DEX_n (n = 0.1, 0.5, 1, 2, 5, 10) polymers

DEX and $NaCNBH_3$ were added to a 1.8 mM solution of PAH:RBITC in borate buffer (0.03 M, pH 8.4). The reaction mixture was kept under magnetic stirring at r.t. and, after 72 h, was loaded into dialysis tubing (cellulose membrane, 14,000 MWCO) that were placed in a 2 L beaker of deionized water. The content of the beaker was gently stirred, recharging with fresh distilled water every 3–4 h over the course of 72 h. Finally, the product was freeze-dried and stored at 4 °C. The PAH:DEX_n polymers were analysed by ^{1}H NMR and IR spectroscopy. The RBITC loading in the PAH:RBITC:DEX_n polymers was confirmed through UV–Vis spectroscopy. The specific syntheses of PAH:RBITC:DEX_n (n = 0.1, 0.5, 1, 2, 5, 10) polymers are reported in the Supporting Material.

2.4. Synthetic procedure for the preparation of PAH:DEX_n PANs

PANs were prepared through a self-assembly process. 0.1 mL of a stock solution (10 mg/mL, Milli-Q water) of PAH:DEX_n polymer (n = 0.1, 0.5, 1, 2, 5, 10) was added to 0.9 mL of PB at pH 7.2 and different concentrations (2, 5, 7, 10 mM).

2.5. BSA entrapment into nanocapsules

0.1 mL stock solution of PAH:DEX_1 polymer (10 mg/mL, Milli-Q water) was mixed with 0.1 mL of different stock solutions of BSA (0.5, 1, 2.5, 5, 7.5, and 10 mg/mL). Then, the mixture was added to PB 5 mM (0.8 mL, pH 7.2). The free BSA was quantified by UV–Vis through analysis of the protein content in the supernatant ($C_{BSA,\ supernatant}$) after centrifugation of the dispersion at 10,000 rpm for 20 min (16,882 g, Fixed angle rotor AFI-RA24-2, AFI SIRENA Refrigerated Centrifuge 0.6L, 230 V, 50 Hz). This analysis was performed using the Novagen® BCA Protein Assay Kit in accordance with the manufacturer's instructions. The absorbance at 562 nm of the resulting solution was measured in a 96-well by using a SpectroStarNano Microplate Reader. The free BSA was calculated as % = ($C_{BSA,\ supernatant}/C_{BSA,\ total}$) * 100.

2.6. Cryogenic electron microscopy (cryo-EM)

PAH:DEX_n NPs were assembled in PB at a final concentration of 1 mg/mL and let stabilize for 30 min. Ultra-thin plasma-treated carbon film TEM grids (Quantifoil holey carbon film R2.2 on 300 Cu Mesh, Electron Microscopy Sciences) were glow discharged (negative, 21 mA, 60 *sec*) and a small volume of the sample (3 μL) was deposited onto them. NP samples were blotted for 1 *sec* (100 % humidity, zero force and zero *sec* wait) and automatically vitrified in liquid ethane by the Vitrobot instrument (ThermoFisher). The imaging was performed with cryo-EM Glacios microscope (ThermoFisher) with magnification from 36 kX to 92 kX. The images obtained from the cryo-EM analysis were analyzed using ImageJ software (https://imagej.nih.gov/ij/index.html).

2.7. Dynamic light scattering (DLS)

DLS measurements were carried out with a Malvern Zetasizer Pro Red Lab Advance instrument in backscattering mode. All studies were performed at a 173° scattering angle with temperature controlled at 25 °C in 1 mL polystyrene cuvettes. Nanoparticles were characterized in terms of size and ζ-potential. Short time measurements were carried out with 3 consecutive measurements for each sample. ζ-potential measurements were performed in auto-mode at 25 °C, with 3 consecutive measurements for each sample.

2.8. Circular dichroism (CD)

CD experiments were performed in a JASCO-1500 spectrophotometer at 20 °C using a quartz cuvette of path length 10 mm. Free BSA and BSA-loaded NCs, with a final BSA concentration of 0.01 mg/mL, were measured in PB 5 mM. Empty NCs were also measured at the same concentration (0.1 mg/mL) as those loaded with BSA. The spectra were recorded in the range of 190–350 nm with a scan rate of 50 nm min^{-1}. Each data point was collected as an average of three accumulation plots at a bandwidth of 1.00 nm.

2.9. Fluorescence correlation spectroscopy (FCS)

FCS was performed with Confocal Microscope Zeiss LSM 880 (Carl Zeiss Gmbh). Acquisition and analysis were controlled by Zen black software. GaASP detector for single fluorescence molecules detection and dynamic characterization was used. Measurements were performed with a Zeiss C-Apochromat 40x, NA 1.2 water immersion objective. Fluorescence was detected in the range 492–754 nm and 571–754 nm, for Atto488-labelled and RBITC-labelled species respectively. Ibidi μ-Slide 8 well ibiTreat chambered coverglass were used. The solutions were diluted in water or PB 5 mM to concentrations four or ten times lower than the original one, resulting in a final volume of 200 μL, in order to avoid the saturation of the detector. QuickFit 3.0 [30] free software was used for FCS data analysis. To fit data the Global Fitting with 2 components 3D Normal Diffusion model was used. The confocal volume was determined using 50 nM Atto488 and 200 nM Rhodamine B solutions. Bovine serum albumin (BSA) was labelled with Atto488 NHS-ester in the following way. BSA (5 mg, 0.0755 μmol, 1 eq) was dissolved in PBS (5 mL) adjusted to pH = 8.3 by using $NaHCO_3$ 0.2 M and incubated overnight with 222 μL of Atto488 NHS-ester DMF solution (1 mg/mL, 0.226 μmol, 3 eq). The crude product was purified by dialysis (10 KDa MWCO) during 48 h. BSA-Atto488 was freeze-dried and a purple solid was obtained (79 % yield).

2.10. Small angle X-ray scattering (SAXS)

SAXS experiments were performed at the Austrian SAXS beamline at the Elettra Synchrotron in Trieste, Italy. The energy of the X-rays was 8 keV, corresponding to a wavelength $\lambda = 1.55$ Å. The sample-to-detector (P1M) distance was adjusted to 1.347 m for the desired *Q*-range

(0.01–0.5 $Å^{-1}$), where Q is the scattering vector with θ one-half of the scattering angle. The specified beam dimensions were 500 × 1500 mm. All samples were measured using the beamline automatic μDrop Sample Changer [31]. Data were acquired in triplicate, by taking 20 images with an exposure time of 10 s in every case. Before and after every sample measurement, the scattering of the correspondent buffer was also acquired. Radiation damage of the samples was checked and only the appropriate waves were selected for the data analysis. The reduction of the primary data was performed using Igor Pro. SAXS data analysis was performed by using the software GENFIT [32]. Two models were adopted to analyse SAXS curves: homogeneous spheres and core–shell spheres, whose radius is considered polydisperse as in previous works [8].

3. Results

3.1. Synthesis of PAH:DEX$_n$ polymers

PAH polymers functionalized with dextran (DEX) were synthesized at different PAH:DEX$_n$ molar ratios (n = 0.1, 0.5, 1, 2, 5, 10) through a reductive amination reaction between the free amine groups in PAH backbone and the terminal aldehyde group present in each DEX chain. The reaction was performed in borate buffer (pH 8.4) with sodium cyanoborohydride as reducing agent, as sketched in Scheme 1.

The reaction mixture was purified by dialysis and then freeze-dried. The detailed synthetic procedures are reported in the Supplementary material Section I. The polymers were analyzed by ^{1}H NMR spectroscopy (Fig. S1) to determine the experimental ratio between the PAH backbone and the DEX polysaccharide after conjugation, *i.e.* the value of n in PAH:DEX$_n$. As detailed in Table S1, the theoretical molar ratios closely matched the experimental ones, suggesting that the reductive amination approach is efficient.

In addition, fluorescent polymers were also prepared by inserting a fluorescent tag on the PAH framework. In particular, PAH was covalently coupled with commercially available Rhodamine B isothiocyanate (RBITC) through thiourea formation in basic conditions. After dialysis and freeze-drying, the resulting fluorescent polymer PAH-RBITC was analyzed through UV–Vis spectroscopy to quantify the amount of fluorophore (Supplementary material Section I for detailed synthesis procedure and characterization). Then, fluorescent PAH:DEX$_n$ polymers (with n = 0.1, 0.5, 1, 2, 5, 10) were synthesized by using PAH-RBITC in place of PAH and following the same synthetic procedure as for non-labelled PAH:DEX$_n$ (Supplementary material, Section I).

3.2. Preparation and characterization of PAH:DEX$_n$ nanoparticles

PAH:DEX$_n$ nanoassemblies were prepared with a simple one-step procedure by mixing synthesized PAH:DEX$_n$ polymers (n = 0.1, 0.5, 1, 2, 5, 10) with PB. An initial screening of PB concentrations was carried out to optimize the NPs formation in terms of size and monodispersity. Furthermore, the effect of ionic strength on NPs synthesis was evaluated adding NaCl to the NPs dispersion to reach a final concentration of NaCl between 0 and 150 mM. In addition, the pH-responsiveness of PAH:DEX$_n$ NPs was evaluated across a wide pH range (3 ≤ pH ≤ 11) by addition of hydrochloric acid or sodium hydroxide to the NPs dispersion. PAH:DEX$_n$ NPs were extensively characterized by dynamic light scattering (DLS) and ζ-potential to determine size, polydispersity, surface charge, and stability over time. Cryogenic electron microscopy (cryo-EM) and synchrotron small angle X-ray scattering (SAXS) also provided key information about their structure and morphology.

A DLS screening in 10 mM PB at pH 7.2 (Table 1) indicate that monodisperse samples are obtained for n = 0.5, 1 and 2, and that the size of the corresponding nanoassemblies decreases as the DEX functionalization increases. In particular, the size of PAH:DEX$_{0.5}$ is 212 nm with PdI 0.02, PAH:DEX$_1$ is 85 nm with PdI 0.04, and PAH:DEX$_2$ is 43 nm with PdI 0.04 (Fig. 1B, Fig. S3). For lower DEX functionalization, *i.e.* PAH:DEX$_{0.1}$, the size of nanoassemblies is 534 nm with PdI 0.17 that is very similar to non-functionalized PAH [8]. Higher PAH:DEX ratios (n = 5 and 10) result in very polydisperse populations, with sizes indicating the presence of free random-coil polymer chains rather than self-assembled species. Furthermore, DLS measurements after 24 h showed that PAH:DEX$_n$ (n = 0.5, 1, and 2) nanoassemblies were more stable and monodisperse than the others over time (Table 1).

Table 1
Size (hydrodynamic diameter, nm) and polydispersity index (PdI) of PAH:DEX$_n$ NPs as measured by DLS, immediately after their synthesis (0 h) and after 24 h, in PB 10 mM, at pH 7.2 and 25 °C. Data were acquired in triplicate.

Polymer samples	Size (nm) ± SD	PdI±SD	Size (nm) ± SD	PdI±SD
	0 h		24 h	
PAH	681 ± 18	0.27 ± 0.06	1060 ± 48	0.46 ± 0.05
PAH:DEX$_{0.1}$	534 ± 10	0.17 ± 0.02	807 ± 32	0.10 ± 0.02
PAH:DEX$_{0.5}$	212 ± 2	0.02 ± 0.02	223 ± 5	0.05 ± 0.04
PAH: DEX$_1$	85 ± 1	0.04 ± 0.01	92 ± 1	0.05 ± 0.02
PAH: DEX$_2$	43 ± 1	0.04 ± 0.01	43 ± 1	0.05 ± 0.02
PAH: DEX$_5$	28 ± 1	0.27 ± 0.01	29 ± 1	0.23 ± 0.02
PAH:DEX$_{10}$	200 ± 165	0.43 ± 0.21	52 ± 35	0.55 ± 0.26

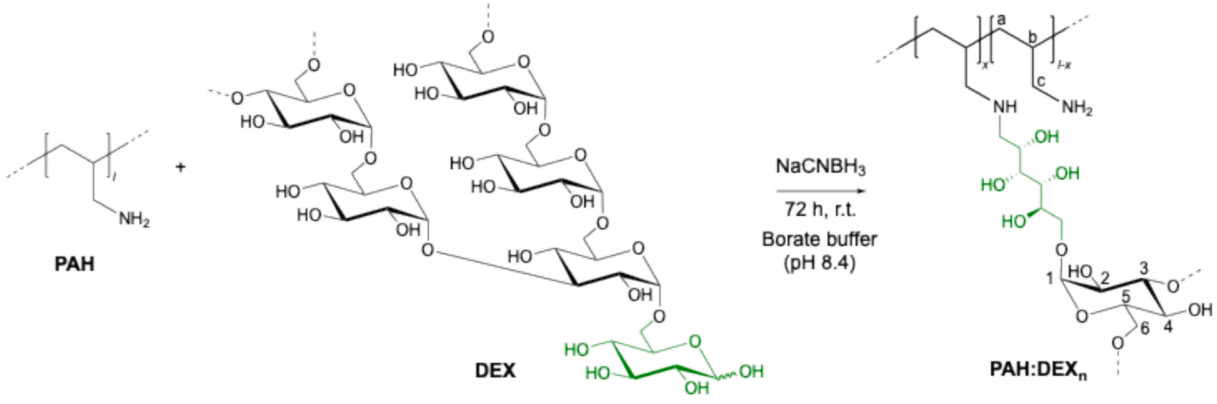

Scheme 1. Synthetic approach for the preparation of PAH:DEX$_n$ polymers, based on reductive amination: the masked aldehyde of the DEX reducing end reacts with the primary amines of the PAH, and the Schiff's base intermediate is reduced in situ with $NaCNBH_3$.

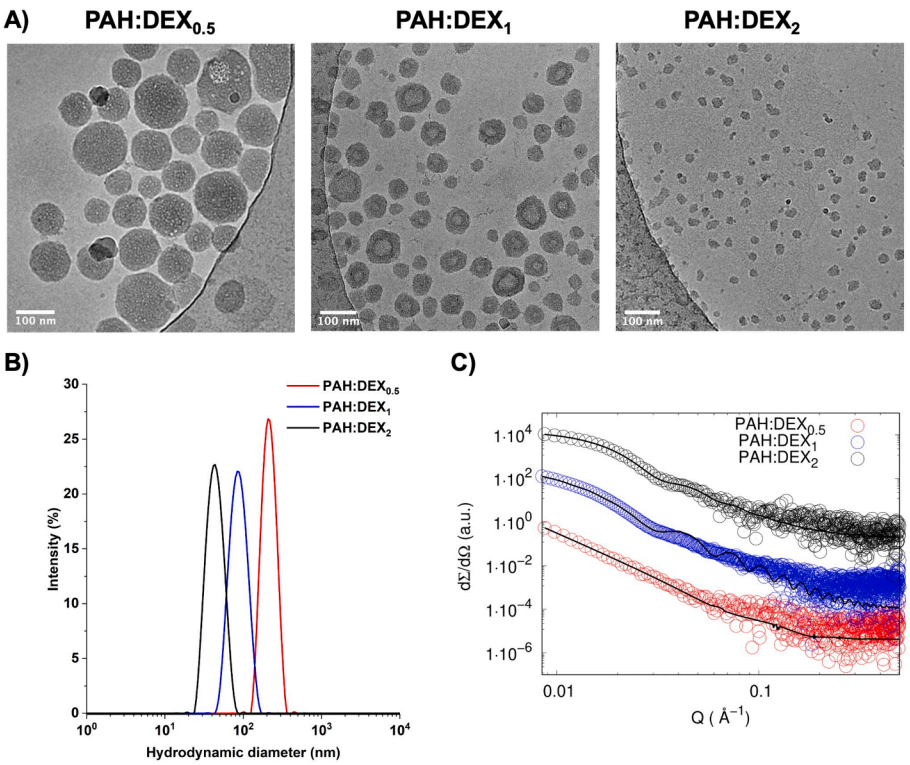

Fig. 1. Analysis of PAH:DEX$_n$ NPs prepared in PB (10 mM, pH 7.2) at 1 mg/mL with different PAH:DEX$_n$ molar ratios (n = 0.5, 1, 2) by A) cryo-EM images; B) DLS intensity-based size distribution; C) SAXS experimental curves (circles) and theoretical fitting (lines), from bottom to top each curve has been scaled by a factor 100 in respect to the lower n molar ratio, for the sake of clarity.

Surface charge measurements (Table S2) show that the ζ-potential decreases from +20 mV for PAH [10] to +0.6 mV for PAH:DEX$_2$ NPs, as consequence of the shielding of positive charges by dextran molecules.

These results have been confirmed by cryo-EM that allowed for a more detailed study by direct visualization of the nanoassemblies in cryogenic conditions. Indeed, cryo-EM images (Fig. 1A and Figs. S4.1, S4.2A, S5A and S6A) reveal an interesting morphological behavior of PAH:DEX in PB 10 mM at different molar ratio of DEX.

In particular, PAH:DEX$_{0.5}$ and PAH:DEX$_2$ clearly appear as spherical nanoparticles (Fig. 1A), PAH:DEX$_5$ and PAH:DEX$_{10}$ appear as very small NPs or random coils (Fig. S4.2A), while PAH:DEX$_1$ showed a completely different morphology. PAH:DEX$_1$ assemble into nanocapsules (NCs) with a core–shell structure formed by an electrodense polymeric layer with an inner core having an electron density similar to the outer space, suggesting an empty core.

A detailed analysis of the cryo-EM images of PAH:DEX$_1$ (Fig. S5A) shows that the NCs population exhibited an average diameter around 70 nm, even though sizes up to 100 nm can be detected. Fig. S5B illustrates the size-distribution histogram. Statistical analysis on the nanocapsules reveals that NCs represent about 66 % of the assemblies and show a polymeric shell with an average thickness of 22 nm, which denotes that the inner core volume of the capsule is relatively small, close to 40 nm in diameter. Additionally, together with the NCs, a small population of nanoparticles below 40 nm can be detected.

The concentration of PB used during the synthesis significantly influenced the formation of PAH:DEX$_1$ NCs as reported in Fig. S6. Cryo-EM images (Fig. S6A) show that NCs start to form at PB 5 mM. A further increase in PB concentration to 10 mM leads to a decrease in the size of NCs. DLS (Fig. S6B and Fig. S6C) confirm these data.

Since cryo-EM provides information on a limited set of nanostructures, SAXS was applied to gain information of a wider population of the nanoassemblies. Cryo-EM results were used to select the fitting model for SAXS experimental data obtained for PAH:DEX$_n$ with n = 0.5, 1, and 2 (Fig. 1). SAXS data corresponding to PAH:DEX$_n$ are shown in Fig. 1C (curves are shifted for visual clarity). A model free approach, aimed to obtain the Guinier gyration radius, suggested that increasing n (number of DEX chains per PAH chain), the average radius decreased. However, since the Q-range where the Guinier approximation is perfectly valid is lower in respect to available experimental set-ups, a theoretical model has been adopted that allows to analyze the whole SAXS spectrum and involves polydisperse spheres, possibly with denser shells, taking advantage of DLS and cryo-EM results. SAXS measurements of PAH:DEX$_{0.5}$ and PAH:DEX$_2$ samples were successfully fitted considering polydisperse spheres with diameters of 180 and 30 nm, respectively, with a polydispersity between 10 and 20 %. On the other hand, SAXS spectrum of PAH:DEX$_1$ could not be quite well analyzed considering just one species in solution. Hence, taking advantage of cryo-EM results, both homogeneous and core–shell spheres were considered to be present in solution for PAH:DEX$_1$ sample. NCs resulted to be ≈60 % of the total species, in good agreement with cryo-EM image. Also, an average diameter of ≈30 nm resulted for NPs, while NCs were characterized by an inner diameter of ≈60 nm and a denser shell of ≈20 nm thickness.

Furthermore, the stability against ionic strength was evaluated. An increase in the size of PAH:DEX$_1$ NCs is observed in PB 10 mM when the ionic strength raises from 0 to 150 mM through the addition of NaCl, as shown in Fig. 2A. The hydrodynamic diameter and PdI of the NCs increases with augmenting NaCl concentration, starting from ≈100 nm in a PB solution (no NaCl), growing to ≈ 150 nm in PB with saline 50–100 mM, and reaching 1115 nm when NaCl concentration is brought to 150 mM. Additionally, DLS measurements were conducted to evaluate the stability of PAH:DEX$_1$ NCs across a wide pH range, from pH 3 to pH 11. These experiments were carried out by adding few microliters of 0.5 M HCl for pH values below 7 or 0.5 M NaOH for pH values above 7. No variation in the scattered intensity of PAH:DEX$_1$ NCs at pH values between 6 and 9 was observed, as shown in Fig. 2B. In this pH region, all PAH chains become saturated with phosphate ions causing their stable complexation and NCs formation. Instead, a decrease in the scattering

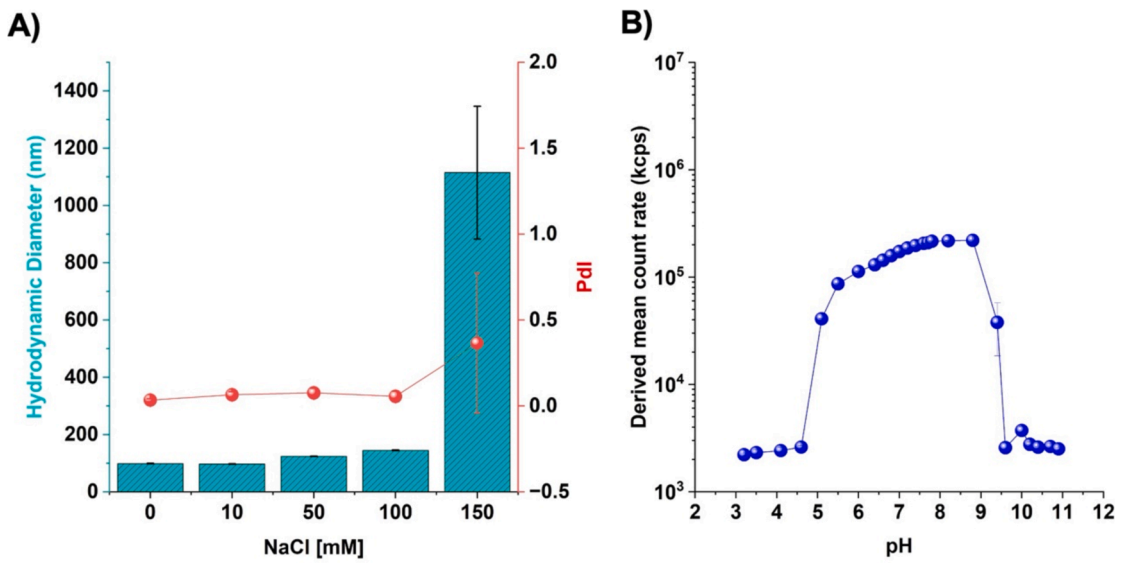

Fig. 2. (A) Hydrodynamic diameter (nm) and PdI of PAH:DEX_1 in PB 10 mM *vs* different molar concentrations of NaCl. (B) Derived mean count rate in kilocounts per second (kcps) of PAH:DEX_1 in PB 10 mM at different pH values.

intensity at acidic pH levels below 6 is likely due to the disassembly of PAH, resulting from the loss of negative charges in phosphate groups at acidic pH. Indeed, at pH < 6, the protonation of PAH is maintained (pK_a PAH ~ 8.92, [33,34]) but the main phosphate species are $H_2PO_4^-$, thus the resulting PAH-phosphate interactions are no longer sufficient to generate stable complexes [35]. Similarly, a disassembly process is observed when the pH is raised above 9. At high pH, the PAH becomes neutral due to the complete deprotonation of amino groups resulting in negligible interactions with phosphate ions, NCs disassembly and lower scattered intensity.

3.3. Entrapment of BSA protein to the PAH:DEX nanocapsules

The potential of PAH:DEX_1 NCs for the encapsulation of biological macromolecules was evaluated by preparing the NCs in presence of BSA at different concentrations (from 0.1 to 1.0 mg/mL). DLS data showed that PAH:DEX_1-$BSA_{0.1}$ NCs exhibit an average diameter of 156 nm with PdI 0.11 ± 0.04, while PAH:DEX_1-BSA_1 NPs a smaller diameter around 48 nm with PdI 0.14 ± 0.02, as clearly visible from intensity-based size distribution graphs (Fig. 3A). Similar results were obtained by SAXS measurements on PAH:DEX_1-$BSA_{0.1}$ and PAH:DEX_1-BSA_1, which are shown in Fig. 3B. When BSA is entrapped at the lower concentration, large NCs are observed, whose diameter is ≈200 nm, including a higher electron density shell with a thickness of ≈20 nm. On the other side, increasing BSA amount until 1 mg/mL, NCs collapse into a population whose average diameter is ≈80 nm. Both SAXS results arise from a theoretical fitting with a noticeable polydispersion, in agreement with cryo-EM. In fact, cryo-EM images were acquired to visualize the entrapment and structural changes at 0.1 mg/mL and 1.0 mg/mL of BSA (Fig. 3C and D). Cryo-EM images show an inner compartment of the NCs with a higher contrast as compared to the regions outside the capsule walls, which was not observed in the absence of protein, thus suggesting that a portion of the BSA is entrapped inside the NCs (Fig. 3C). Conversely, at 1 mg/mL of BSA, relatively small (≈25 nm) nanoparticles are formed (Fig. 3D).

The entrapment efficiency at different concentrations of BSA (ranging from 0.05 to 1.0 mg/mL) in PAH:DEX_1 was evaluated in PB 5 mM (pH 7.2, 20 °C) using the Novagen® BCA Protein Assay Kit, immediately after mixing (t = 0 min), as shown in Fig. S7 (blue bars). The bar plot indicates that, when the BSA concentration is below 0.1 mg/mL, no free protein is detected in the supernatant. However, as the BSA concentration increases to 1 mg/mL, complete encapsulation of the protein cannot be achieved. As DLS showed that the NCs disassemble at pH below 6 (Fig. 2B), the release of BSA was studied at pH 4.5 using the Novagen® BCA Protein Assay Kit. As shown in Fig. S7 (orange bars), at t = 0 min, the disassembly of the NCs and the release of the protein occur immediately, reaching a plateau when the concentration exceeds 0.5 mg/mL. Furthermore, this trend was confirmed even at t = 60 min indicating no changes in the amount of protein present in the supernatant, reinforcing the conclusion that the release is immediate, as reported in Fig. S8.

DLS (Fig. S9A) provides a clear correlation between pH variation and the disassembly of the NCs. This visual transition is evident in Fig. S9B that shows the sample at pH 7.2 on the left and at pH 4.5 on the right. The solution appears opalescent at pH 7.2, indicating the presence of intact NCs. However, when the pH is adjusted to 4.5, the solution becomes clear, indicating the complete disassembly of the NCs. These observations confirm that the lower pH environment effectively triggers the disassembly of the PAH:DEX_1-$BSA_{0.1}$ NCs, releasing the entrapped BSA and resulting in the disruption of the NCs.

Far-UV CD spectroscopy was applied to further evaluate the entrapment/release process, but focusing on the cargo, *i.e.* BSA (Fig. 4A and B), since no meaningful CD signal was observed for the empty NCs as reported in Fig. S10. In particular, the aim of the CD experiments was to monitor the structural changes of BSA when entrapped in PAH:DEX_1 NCs at pH 7.4, and to evaluate its stability and release at pH 4.5 [36]. Fig. 4A shows that free BSA at pH 7.4 *vs* BSA mixed with PAH:DEX_1 NCs (at the same pH) provide different CD spectra with a significant change in the relative intensity of the two minimums of the free BSA. These CD spectra demonstrate two distinctive BSA structures, and hence confirm BSA entrapment. Specifically, the encapsulated BSA shows a decrease in the intensity of the bands at 190 nm and 208 nm, while the band at 220 nm remains unchanged in intensity, but it exhibits a slight red shift. The changes in both bands suggest a loss of conformation of BSA through the interaction with the PAH:DEX polymer. These changes are due to the modification of BSA secondary structures induced by its entrapment in the NCs. Indeed, lowering the pH from 7.4 to 4.5, the encapsulated BSA display similar CD spectra to the free BSA (Fig. 4B) with a comparable intensity ratio between the two minima, suggesting that BSA is released from the NCs at this pH, recovering the initial conformation. The peak at 220 nm becomes less negative when the pH decreases, in agreement with literature data [37].

To have an additional proof of the entrapment capability of proteins, fluorescence correlation spectroscopy (FCS) studies were carried out

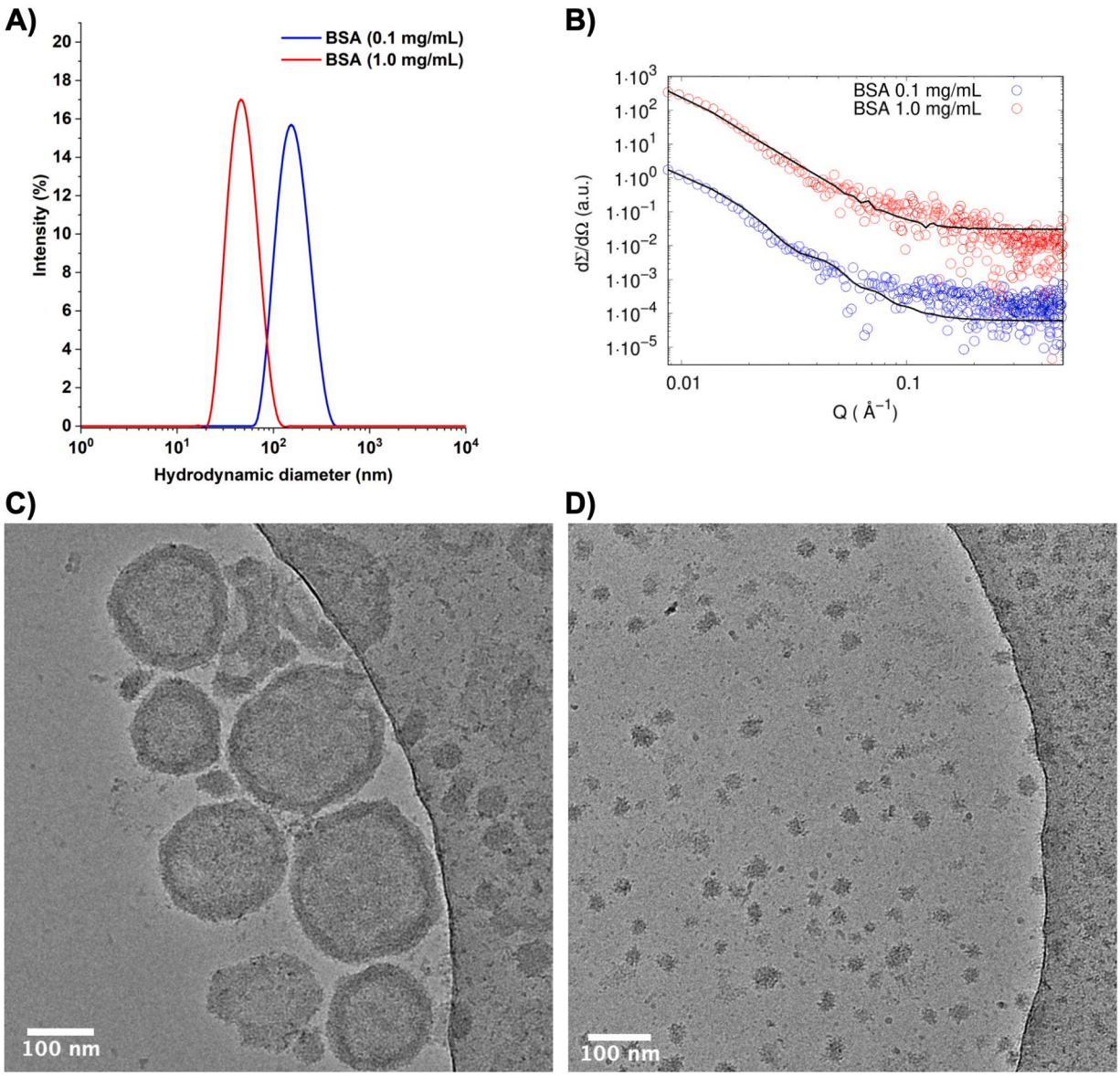

Fig. 3. Entrapment of BSA (0.1 or 1.0 mg/mL) in PAH:DEX$_1$ (1 mg/mL in PB 5 mM, pH 7.2). (A) Size distribution based on DLS intensity; (B) SAXS experimental curves (circles) and theoretical fitting (lines); SAXS curve at higher BSA concentration has been shifted by a factor 100 for clarity; Cryo-EM images with (C) 0.1 mg/mL of BSA, and (D) 1 mg/mL of BSA.

(Fig. 4C and D). FCS allows to measure the diffusion coefficient of fluorescently labelled molecules. BSA was labelled with Atto488 through a standard protocol and its diffusion coefficient was measured before and after entrapment in the PAH:DEX$_1$ NCs. The diffusion coefficient of the protein decreases after encapsulation from 31.6 ± 0.8 μm^2/s to 3.3 ± 0.3 μm^2/s, which means that the protein diffuses in a similar way as the NCs. To probe that, PAH-RBITC:DEX$_1$ NCs without BSA were prepared (Fig. 4D). Their diffusion coefficient was measured, which resulted in the same order of magnitude as the one observed for the encapsulated protein. When the ionic strength was increased over 150 mM of NaCl (Fig. S11) or the pH decreased to 5 (Fig. 4C), the diffusion time of the entrapped protein decreased to values of free protein, indicating a disassembly of the NCs and the BSA protein release.

4. Discussion

The preparation of PAH:DEX PANs requires the controlled synthesis of pristine polymers, which has been carried out through a reductive amination reaction profiting of the masked aldehyde at the terminal glucoside in the DEX chains. This strategy allows for a significant chemical control (PAH:DEX$_n$, with n = 0.1, 0.5, 1, 2, 5, 10; see Supplementary material. Section I). Due to the chemoselectivity of the reaction, free amine groups in PAH backbone react with the unique hemiacetal at DEX terminal end affording the corresponding Schiff base that is in situ reduced to the corresponding secondary amine by $NaCNBH_3$. The reaction is easy to perform and straightforward, as well as the purification process that is based on dialysis *vs* water. In addition, it ensures that a single DEX chain reacts independently from another chain and specifically, as the hydroxyl groups are not involved in the bond formation. The high chemical control allows for obtaining different PAH:DEX ratios. PAH:DEX$_n$ PANs show a richer assembly behavior than PANs prepared with PAH or with PAH modified with oleic acid or PEG [10,18,20]. The size and the morphology of PAH:DEX$_n$ assemblies are modulated by changing the molar ratio of DEX and PAH. In PB 10 mM, PAH:DEX$_n$ with densities of DEX chains below 1 per PAH chain assembles forming PANs, as PAH does. In fact, a density of DEX chains below 1 implies that not all chains are modified with DEX, thus the polymers can interact among themselves as unmodified PAH chains.

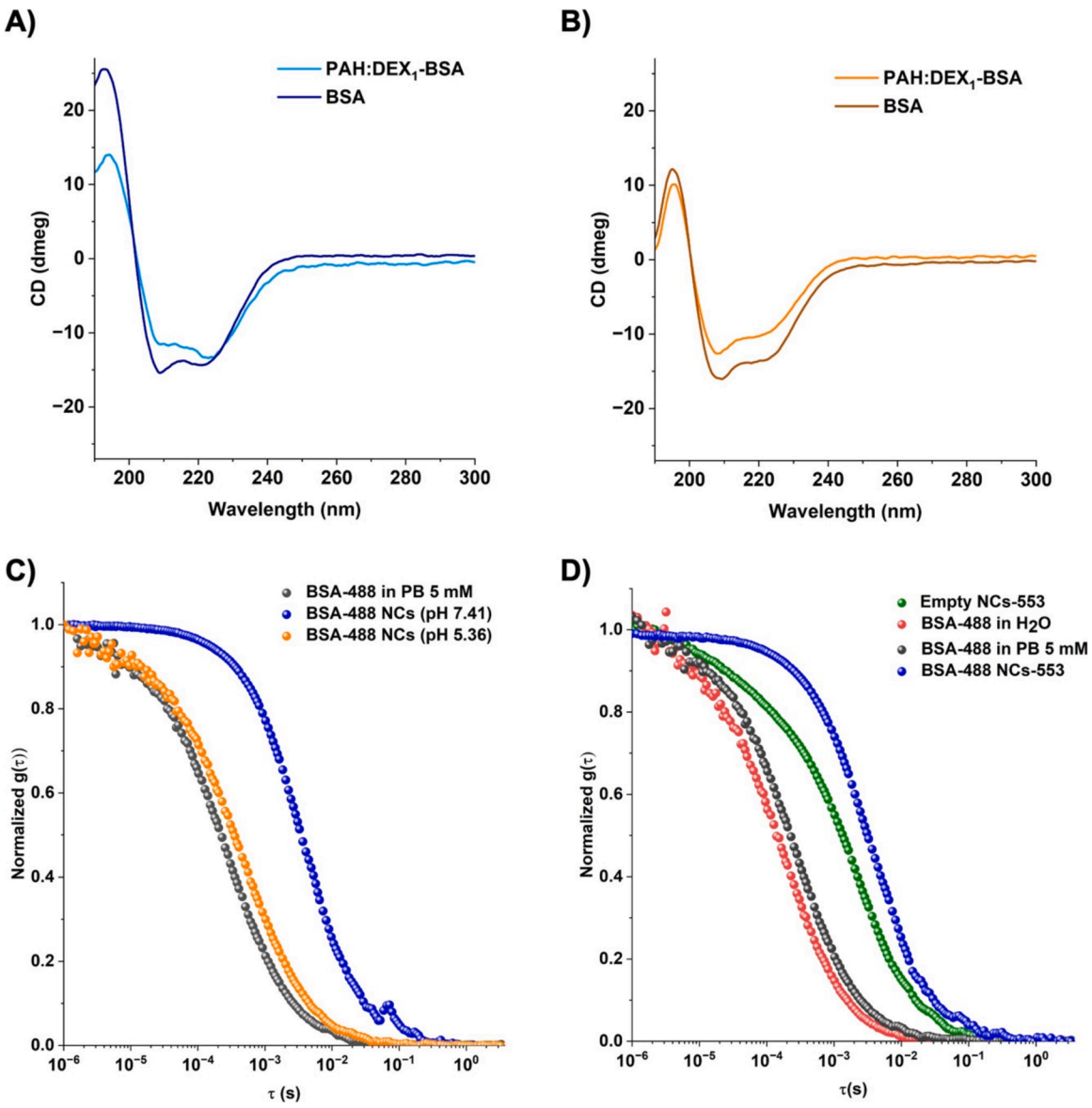

Fig. 4. CD spectra of PAH:DEX_1-BSA (0.1 mg/mL) and free BSA (0.1 mg/mL) in PB 5 mM at pH 7.4 (A) and at pH 4.5 (B). Autocorrelation curves obtained from FCS using Atto488-labelled BSA (BSA-488) for (C) BSA-488 in PB 5 mM, after forming PAH:DEX_1 NCs at pH 7.4 and pH 5.4; (D) Empty NCs formed with RBITC-labelled PAH:DEX_1 (NC-553), the same NCs with BSA-488, and free BSA-488 in water and PB 5 mM.

The interaction of PAH chains free of DEX with PAH:DEX_n at densities below 1 can take place randomly among amines of both chains, except for the regions of PAH:DEX_n that are sterically protected by DEX. DEX is a large and branched polysaccharide attached from one point to the PAH. A non-modified PAH can interact with the PAH:DEX_n in PB from any direction except from the side protected by DEX. For the case of PAH:DEX_n with $n = 0.1$, a PAH chain is most likely to encounter another PAH chain than a PAH functionalized with DEX. In these conditions, the assembly is very similar to the PAH, resulting in particles with size and morphology similar to PANs synthesized with unmodified PAH, as shown in cryo-EM images. However, when a PAH:DEX chain assembles, DEX must be placed on the surface of the nanoparticle otherwise the interaction among PAH chains would not be optimal, since if DEX were inside the nanoparticle it would sterically shield the interaction of amines from one chain to another through the phosphate ions, acting as a barrier.

In the case of PAH:DEX_n with $n = 1$ (approximately one dextran polysaccharide per PAH chain), each PAH:DEX polymer can only interact with other PAH:DEX chains. The assembly can hence proceed by the side if the DEX chains do not impose steric constrains or two PAH chains come together from opposite directions with the dextran chains on their back (Fig. 5). When this occurs, the assembly cannot grow further in thickness as the PAH chains are trapped between dextran layers. The assembly continues sidewise, or it is stopped if DEX imposes restrictions for lateral growth. In one case, nanocapsules are formed; in the other case, small nanoparticles. The size of the DEX is smaller than the side of the PAH chain to which is attached, and this allows the PAH:DEX chains to assembly side by side. In analogy to a lipid bilayer, we assume that they close on themselves forming a sort of polymer vesicle. Reasonably, the capsule formation is only possible when the DEX chains are located both on the external and internal surface of the assemblies. The thickness of the NCs must be at most the thickness of two PAH:DEX chains in the conditions for the assembly and DEX must be present in both the inner and external surface, extended for around 20 nm. This is also the size of small nanoparticles, which makes us think that the nanoparticles are formed by two PAH:DEX chains, which were not able to growth laterally. It could also be possible that one or two additional chains of PAH:DEX could be present, consequently forming the complex

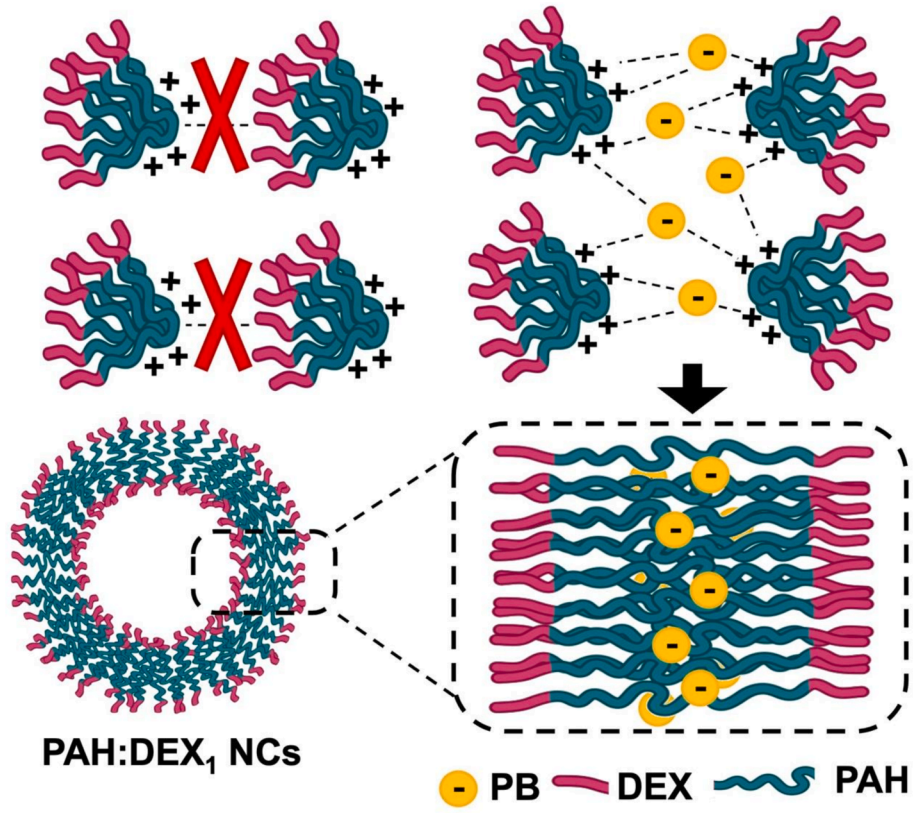

Fig. 5. Sketch of the self-assembly mechanism of PAH:DEX_1 into nanocapsules. The sketch shows how DEX poses constrain for the assembly that leads to the interaction of PAH:DEX chains only when the PAH backbone of two chains are facing one to the other. The assembly can grow laterally when the positive charges in the complex can interact with the charged backbone of other PAH:DEX. The negative charges are intended to be the $H_2PO_4^-$ / HPO_4^{2-} ions; the positive charges are intended to be the protonated amino groups of the PAH.

in such a way that the DEX chains do not allow for further growth of the assembly.

More insight on the structural features of PAH:DEX_n (n = 0.5, 1, 2) are given by the surface charge measurements in PB 10 mM at pH 7.2 (Table S2), which corroborate the successful functionalization of DEX on PAH. Notably, there is a significant decrease of the positive surface charge in PAH:DEX_n NPs as the amount of DEX on PAH increases. The DEX polysaccharide shields the PAH positive charges, bringing ζ-potential close to 0 mV in the measuring conditions. This result also confirms that the DEX chains are mainly exposed to the bulk solution, similarly to what happened when PAH was functionalized with PEG [10].

The absence of nanoparticle formation for $n > 2$ is probably due to the large screening of charged of PAH by the two DEX moieties per PAH molecule, which prevents the interaction of unmodified PAH segments with the phosphate ions imposing steric constraints for particle formation and growth. When the number of DEX per PAH is increased over 5, the interaction between chains is limited by steric restrictions. They cannot assemble resulting in single chain nanoparticles when segments of PAH can interact within a single chain through phosphate ions or when the number of DEX chains does not allow for this interaction the PAH:DEX chains remain unperturbed, and no nanoparticle is formed.

The pH-responsiveness of PAH:DEX_1 NCs was evaluated across a pH range from 3 to 11. As shown in Fig. 2B, the nanocapsules are stable in a $6 < pH < 9$ range and disassemble at $pH < 6$ or $pH > 9$. The protonation of the phosphate groups at acidic pH, as well as the deprotonation of amino groups at $pH > 9$, leads to the disassembly of the NCs. In addition, the increase in size with ionic strength (>150 mM), shown in Fig. 2A, is probably due to the decrease in repulsive interactions among the PAH chains that facilitate grows of the particle, while the attractive interaction between the amines of PAH and the phosphate ions are still present. Further increases in the ionic strength weakens the phosphate amine interactions and capsules dissolve. The above data indicate that the nanocapsules show a narrow size distribution and should disassemble in conditions of pH displayed in late endosomes but not during circulation into the bloodstream, which makes them an interesting and innovative system for the encapsulation and the delivery of large therapeutics and biologics, such as proteins and nucleic acids. In order to demonstrate that these capsules can be exploited to encapsulate hydrophilic biomolecules, BSA has been used as a model protein. Measuring by FCS the diffusion time of the fluorescently labelled NCs and the free labelled BSA, in comparison with the PAH:DEX_1-$BSA_{0.1}$, indicate that most of BSA is encapsulated and diffuses with the capsules as it has a very similar diffusion time to the empty NCs. FCS data show that, when encapsulated, the protein diffuses with the capsule and can be easily released by a decrease in pH to values below 4.5, as shown in Fig. 4C and D.

When the final concentration of BSA was 0.1 mg/mL, the formation of the nanocapsules with entrapped protein has been visualized by cryo-EM (Fig. 3C). The images show a contrast in the inner volume of the capsules, which is not observed in the absence of the protein (Fig. 1A and Fig. 6SA). Increasing BSA concentration to 1.0 mg/mL led to the formation of small nanoparticles without the characteristic core–shell structure (Fig. 3D). Since BSA is added to PAH:DEX before the addition of PB, it is possible that the protein forms a complex with the polymer before the nanocapsule formation. The structure of the capsules with proteins may be different from the empty capsules and is the subject of further studies.

5. Conclusions

Novel supramolecular polyamine phosphate nanoassemblies, *i.e.* glyconanocapsules, have been here reported for the first time, and have

been obtained after controlled chemical modification of PAH polymer with DEX polysaccharide through a reductive amination-based process that allows for a controlled DEX conjugation to the polyamine backbone. Varying the number of DEX chains attached to PAH chains and inducing self-assembly through the addition of PB provide a palette of polymer assemblies. At low DEX densities, the formation of dense polymer nanoparticles takes place. When the number of DEX chains per PAH molecule becomes 1, the PAH:DEX polymers form capsules in the 100 nm range. At larger densities of DEX, single chain nanoparticles are formed, or the polymers do not form nanostructures at all. The rich behavior of DEX-modified PAH can be explained by the steric constrains in the assembly imposed by the bulky DEX. As the number of chains of DEX per PAH increases, the growth of the assemblies in the regions of the PAH chains is limited by the shielding effect of the DEX. When all chains are functionalized with one DEX chain, the interaction of two PAH:DEX_1 polymers with the DEX chain behind limits the growth from the DEX sides and the growth can only proceed laterally, forming capsules. Dextran densities below 1 impose less constrains to self-assembly forming dense particles with variable size and with DEX located on the surface. Larger DEX densities prevent interactions between polymer chains, resulting in single or few chain nanoparticles or the absence of particle formation, if the density of DEX is too high. PAH:DEX_1 capsules are pH-responsive systems capable of encapsulating macromolecules and releasing them at acid pH comparable with late endosomal pH values. The functional behavior of this responsive glyconanocapsules was demonstrated with FCS and CD with the entrapment and release of BSA as a model protein. Cryo-EM was able to visualize the structural characteristics of the nanocapsules and the interactions with the entrapped BSA protein, in combination with SAXS.

The results of this work show that the branched nature of DEX together with a strict control of chemical functionalization allows for the generation of alternative novel PAH-based nanoassemblies in phosphate buffer, *i.e.* nanocapsules, which were not previously observed for PEG-functionalized PAH [10]. It is here demonstrated that the completely different supramolecular organization driven by DEX chains as capsules offers the possibility to encapsulate biologics, such as proteins, and to control their release by pH modulation. These glycoNCs are thus interesting nanoscale carriers with supramolecular organization and smart pH responsiveness, which could be exploited for intracellular delivery of therapeutics. The optimization of the systems in terms of stability to higher ionic strengths by using higher molecular weight DEX is ongoing. Furthermore, the biocompatibility and targeting properties of DEX towards carbohydrate binding proteins expressed at cell surface [38] pave the way for further investigations of targeted drug delivery applications through glycoNCs.

Funding sources

The financial support provided by the MUR – Dipartimenti di Eccellenza 2023-2027 (DICUS 2.0, CUP: B97G22000740001) to the Department of Chemistry "Ugo Schiff" of the University of Florence is acknowledged. This work was performed under the Maria de Maeztu Units of Excellence Program from the Spanish State Research Agency – Grant no. MDM-2017-0720. S.E.M. thanks the PID2020-114356RB-I00 project from the Ministry of Science and Innovation of the Government of Spain. S.E.M and M.M. acknowledge support from the European Union's Horizon 2020 research and innovation programme under the Marie Skłodowska-Curie grant agreement 101008072 (H2020-MSCA-RISE-2020 Project SUPRO-GEN "Supramolecular Polyamine Gene Vectors for Cancer Therapy"). F.M. and M.M. thank for funding the European Union - NextGenerationEU programme in the context of the National Recovery and Resilience Plan, Mission 4, Component 2, Investment 1.5, ECS00000017, THE "Tuscany Health Ecosystem" - Spoke 4 "Nanotechnologies for diagnosis and therapy", CUP: B83C22003920001. M.M. also acknowledge co-funding from the European Union - NextGenerationEU programme in the context of the National Recovery and Resilience Plan, Mission 4, Component 2, Investment 1.4, CN00000041, CN3 "National Center for Gene Therapy and Drugs based on RNA Technology" - Spoke 5 "Inflammatory and Infectious Diseases", CUP: B13C22001010001. M.G.O. thanks for funding the European Union – NextGenerationEU in the context of the National Recovery and Resilience Plan, Mission 4, Component 2, Investment 1.5, ECS00000041, VITALITY "Innovation, digital-ization and sustainability for the diffused economy in Central Italy", Spoke 5 "Environmental, economic and social sustainability of living and working environments", CUP: I33C22001330007. S.G.R. and H.R. thank the Agencia Nacional de Promoción Científica y Tecnológica (AN-PCyT), Argentina, for the project PICT-2019-3185.

CRediT authorship contribution statement

Aharon Steffè: Visualization, Validation, Methodology, Investigation, Formal analysis, Data curation. **Francesca Milano:** Visualization, Validation, Methodology, Investigation, Formal analysis, Data curation. **Santiago Giménez Reyes:** Investigation, Formal analysis, Data curation. **Francesca Buco:** Visualization, Validation, Methodology, Investigation, Formal analysis, Data curation. **Riccardo Leonetti:** Methodology, Investigation. **Yessica Roque-Diaz:** Investigation, Data curation. **Sofia Zuffi:** Investigation. **Paolo Di Gianvincenzo:** Supervision, Methodology, Investigation. **Angela Roberta Cortese:** Investigation. **Hernan Ritacco:** Supervision. **Patrizia Andreozzi:** Writing – original draft, Supervision, Methodology, Investigation, Conceptualization. **Maria Grazia Ortore:** Writing – review & editing, Writing – original draft, Visualization, Supervision, Funding acquisition, Conceptualization. **Sergio E. Moya:** Writing – review & editing, Writing – original draft, Supervision, Project administration, Funding acquisition, Conceptualization. **Marco Marradi:** Writing – review & editing, Writing – original draft, Supervision, Funding acquisition, Conceptualization.

Declaration of competing interest

The authors declare that they have no known competing financial interests or personal relationships that could have appeared to influence the work reported in this paper.

Acknowledgements

We acknowledge Elettra Sincrotrone Trieste for providing access to its synchrotron radiation facilities and we thank Heinz Amenitsch for assistance in using Austrian SAXS beamline. The authors acknowledge the CERIC-ERIC Consortium for the access to experimental facilities.

Appendix A. Supplementary data

Supplementary data to this article can be found online at https://doi.org/10.1016/j.jcis.2024.12.074.

Data availability

Data will be made available on request.

References

[1] J. Wahlich, A. Desai, F. Greco, K. Hill, A.T. Jones, R.J. Mrsny, G. Pasut, Y. Perrie, F. P. Seib, L.W. Seymour, I.F. Uchegbu, Nanomedicines for the delivery of biologics, Pharmaceutics 11 (2019) 210, https://doi.org/10.3390/pharmaceutics11050210.
[2] M.J. Mitchell, M.M. Billingsley, R.M. Haley, M.E. Wechsler, N.A. Peppas, R. Langer, Engineering precision nanoparticles for drug delivery, Nat. Rev. Drug Discov. 20 (2021) 101–124, https://doi.org/10.1038/s41573-020-0090-8.
[3] W. Gao, J.M. Chan, O.C. Farokhzad, pH-responsive nanoparticles for drug delivery, Mol. Pharm. 7 (2010) 1913–1920, https://doi.org/10.1021/mp100253e.
[4] D. Patra, B. Basheer, R. Shunmugam, pH-responsive materials: properties, design, and applications, in: E. N. Zare, P. Makvandi (Eds.), Stimuli-Responsive Materials

for Biomedical Applications, ACS Symposium Series, 2023, pp. 145–179. doi: 10.1021/bk-2023-1436.ch007.
[5] S. Chatterjee, E. Kon, P. Sharma, D. Peer, Endosomal escape: a bottleneck for LNP-mediated therapeutics, Proc. Natl. Acad. Sci. U.S.A. 121 (2024), https://doi.org/10.1073/pnas.2307800120.
[6] S.E. Herrera, M.L. Agazzi, E. Apuzzo, M.L. Cortez, W.A. Marmisollé, M. Tagliazucchi, O. Azzaroni, Polyelectrolyte-multivalent molecule complexes: physicochemical properties and applications, Soft Matter 19 (2023) 2013–2041, https://doi.org/10.1039/d2sm01507b.
[7] P. Andreozzi, E. Diamanti, K.R. Py-Daniel, P.R. Cáceres-Vélez, C. Martinelli, N. Politakos, A. Escobar, M. Muzi-Falconi, R. Azevedo, S.E. Moya, Exploring the pH Sensitivity of Poly(allylamine) Phosphate Supramolecular Nanocarriers for Intracellular siRNA Delivery, ACS Appl. Mater. Interfaces 9 (2017) 38242–38254, https://doi.org/10.1021/acsami.7b11132.
[8] P. Andreozzi, C. Ricci, J.E.M. Porcel, P. Moretti, D. Di Silvio, H. Amenitsch, M. G. Ortore, S.E. Moya, Mechanistic study of the nucleation and conformational changes of polyamines in presence of phosphate ions, J. Colloid Interface Sci. 543 (2019) 335–342, https://doi.org/10.1016/j.jcis.2019.02.040.
[9] V.E. Cuenca, H. Martinelli, M.D.L.A. Ramirez, H.A. Ritacco, P. Andreozzi, S. E. Moya, Polyphosphate poly(amine) nanoparticles: self-assembly, thermodynamics, and stability studies, Langmuir 35 (2019) 14300–14309, https://doi.org/10.1021/acs.langmuir.9b02636.
[10] P. Andreozzi, C. Simó, P. Moretti, J.M. Porcel, T.U. Lüdtke, M. de los A. Ramirez, L. Tamberi, M. Marradi, H. Amenitsch, J. Llop, M.G. Ortore, S.E. Moya, Novel core–shell polyamine phosphate nanoparticles self-assembled from pegylated poly (allylamine hydrochloride) with low toxicity and increased in vivo circulation time, Small 17 (2021), https://doi.org/10.1002/smll.202102211.
[11] S.E. Herrera, M.L. Agazzi, M.L. Cortez, W.A. Marmisollé, M. Tagliazucchi, O. Azzaroni, Polyelectrolyte–ion complexes as stimuli-responsive systems for controlled drug delivery, in: O. Azzaroni, M. Conda-Sheridan (Eds.), Supramolecular Nanotechnology: Advanced Design of Self-Assembled Functional Materials, Wiley, 2023, pp. 729–764, https://doi.org/10.1002/9783527834044.ch27.
[12] M.L. Agazzi, S.E. Herrera, M.L. Cortez, W.A. Marmisollé, M. Tagliazucchi, O. Azzaroni, Insulin delivery from glucose-responsive, self-assembled, polyamine nanoparticles: smart “sense-and-treat” nanocarriers made easy, Chem. - A Euro. J. 26 (2020) 2456–2463, https://doi.org/10.1002/chem.201905075.
[13] L. Gholami, A. Mahmoudi, R. Kazemi Oskuee, B. Malaekeh-Nikouei, An overview of polyallylamine applications in gene delivery, Pharm. Dev. Technol. 27 (2022) 714–724, https://doi.org/10.1080/10837450.2022.2107014.
[14] D. Di Silvio, M. Martínez-Moro, C. Salvador, M. de los Angeles Ramirez, P. R. Caceres-Velez, M.G. Ortore, D. Dupin, P. Andreozzi, S.E. Moya, Self-assembly of poly(allylamine)/siRNA nanoparticles, their intracellular fate and siRNA delivery, J. Colloid Interf. Sci. 557 (2019) 757–766, https://doi.org/10.1016/j.jcis.2019.09.082.
[15] C. Simo, C. Salvador, P. Andreozzi, V. Gomez-Vallejo, G. Romero, D. Dupin, J. Llop, S.E. Moya, Positron emission tomography studies of the biodistribution, translocation, and fate of poly allyl amine-based carriers for sirna delivery by systemic and intratumoral administration, Small 19 (2023) e2304326, https://doi.org/10.1002/smll.202304326.
[16] A.E. Pegg, Toxicity of polyamines and their metabolic products, Chem. Res. Toxicol. 26 (2013) 1782–1800, https://doi.org/10.1021/tx400316s.
[17] J.H. Yu, J. Huang, H.L. Jiang, J.S. Quan, M.H. Cho, C.S. Cho, Guanidinylated poly (allyl amine) as a gene carrier, J. Appl. Polym. Sci. 112 (2009) 926–933, https://doi.org/10.1002/app.29440.
[18] C. Salvador, P. Andreozzi, G. Romero, I. Loinaz, D. Dupin, S.E. Moya, Self-assembled oleic acid-modified polyallylamines for improved siRNA transfection efficiency and lower cytotoxicity, ACS Appl. Bio Mater. 6 (2023) 529–542, https://doi.org/10.1021/acsabm.2c00845.
[19] G.P. Tang, J.M. Zeng, S.J. Gao, Y.X. Ma, L. Shi, Y. Li, H.-P. Too, S. Wang, Polyethylene glycol modified polyethylenimine for improved CNS gene transfer: effects of PEGylation extent, Biomaterials 24 (2003) 2351–2362, https://doi.org/10.1016/S0142-9612(03)00029-2.
[20] P. Perez Schmidt, T. Luedtke, P. Moretti, P. Di Gianvincenzo, M. Fernandez Leyes, B. Espuche, H. Amenitsch, G. Wang, H. Ritacco, L. Polito, M.G. Ortore, S.E. Moya, Assembly and recognition mechanisms of glycosylated PEGylated polyallylamine phosphate nanoparticles: a fluorescence correlation spectroscopy and small angle X-ray scattering study, J. Colloid Interface Sci. 645 (2023) 448–457, https://doi.org/10.1016/j.jcis.2023.04.136.
[21] D. Jiang, A.K. Salem, Optimized dextran–polyethylenimine conjugates are efficient non-viral vectors with reduced cytotoxicity when used in serum containing environments, Int. J. Pharm. 427 (2012) 71–79, https://doi.org/10.1016/j.ijpharm.2011.10.032.
[22] W. Tseng, C. Tang, T. Fang, The role of dextran conjugation in transfection mediated by dextran-grafted polyethylenimine, J. Gene Med. 6 (2004) 895–905, https://doi.org/10.1002/jgm.572.
[23] J. Zhao, C. Wang, P. Zhao, X. Wen, C. Lin, Bioreducible dextran–polyethylenimine conjugates regulate transgene expression distribution in vivo, J. Mater. Chem. B 3 (2015) 1529–1536, https://doi.org/10.1039/C4TB01927J.
[24] M. Ibrahim, E. Ramadan, N.E. Elsadek, S.E. Emam, T. Shimizu, H. Ando, Y. Ishima, O.H. Elgarhy, H.A. Sarhan, A.K. Hussein, T. Ishida, Polyethylene glycol (PEG): the nature, immunogenicity, and role in the hypersensitivity of PEGylated products, J. Controlled Release 351 (2022) 215–230, https://doi.org/10.1016/j.jconrel.2022.09.031.
[25] A. Luanda, V. Badalamoole, Past, present and future of biomedical applications of dextran-based hydrogels: a review, Int. J. Biol. Macromol. 228 (2023) 794–807, https://doi.org/10.1016/j.ijbiomac.2022.12.129.
[26] M. Naessens, A. Cerdobbel, W. Soetaert, E.J. Vandamme, Leuconostoc dextransucrase and dextran: production, properties and applications, J. Chem. Technol. Biotechnol. 80 (2005) 845–860, https://doi.org/10.1002/jctb.1322.
[27] S.R. Van Tomme, W.E. Hennink, Biodegradable dextran hydrogels for protein delivery applications, Exp. Rev. Med. Dev. 4 (2007) 147–164, https://doi.org/10.1586/17434440.4.2.147.
[28] S. Liu, J. Tang, F. Ji, W. Lin, S. Chen, Recent advances in zwitterionic hydrogels: preparation, property, and biomedical application, Gels 8 (2022) 46, https://doi.org/10.3390/gels8010046.
[29] M. Bashari, C. Lagnika, D. Ocen, H. Chen, J. Wang, X. Xu, Z. Jin, Separation and characterization of dextran extracted from deteriorated sugarcane, Int. J. Biol. Macromol. 59 (2013) 246–254, https://doi.org/10.1016/j.ijbiomac.2013.04.046.
[30] J.L. Jan Wolfgang Krieger, QuickFit 3.0. A data evaluation application for biophysics, 2015.
[31] R. Haider, B. Sartori, A. Radeticchio, M. Wolf, S.D. Zilio, B. Marmiroli, H. Amenitsch, MDrop: a system for high-throughput small-angle X-ray scattering measurements of microlitre samples, J. Appl. Crystallogr. 54 (2021) 132–141, https://doi.org/10.1107/S1600576720014788.
[32] F. Spinozzi, C. Ferrero, M.G. Ortore, A. De Maria Antolinos, P. Mariani, GENFIT: Software for the analysis of small-angle X-ray and neutron scattering data of macro-molecules in solution, J. Appl. Crystallogr. 47 (2014) 1132–1139, https://doi.org/10.1107/S1600576714005147.
[33] B.N. Dickhaus, R. Priefer, Determination of polyelectrolyte pKa values using surface-to-air tension measurements, Colloids Surf. A Physicochem. Eng. Asp 488 (2016) 15–19, https://doi.org/10.1016/j.colsurfa.2015.10.015.
[34] V.E. Cuenca, H. Martinelli, M. de los A. Ramirez, H.A. Ritacco, P. Andreozzi, S. E. Moya, Polyphosphate poly(amine) nanoparticles: self-assembly, thermodynamics, and stability studies, Langmuir 35 (2019) 14300–14309, https://doi.org/10.1021/acs.langmuir.9b02636.
[35] S.E. Herrera, M.L. Agazzi, M.L. Cortez, W.A. Marmisollé, M. Tagliazucchi, O. Azzaroni, Polyamine colloids cross-linked with phosphate ions: towards understanding the solution phase behavior, ChemPhysChem 20 (2019) 1044–1053, https://doi.org/10.1002/cphc.201900046.
[36] D. Corrêa, C. Henrique, I. Ramos, D.H.A. Corrêa, C.H.I. Ramos, The use of circular dichroism spectroscopy to study protein folding, form and function, Afr. J. Biochem. Res. 3 (2009) 164–173. http://www.academicjournals.org/AJBR.
[37] N. El Kadi, N. Taulier, J.Y. Le Huérou, M. Gindre, W. Urbach, I. Nwigwe, P.C. Kahn, M. Waks, Unfolding and refolding of bovine serum albumin at acid pH: Ultrasound and structural studies, Biophys J 91 (2006) 3397–3404, https://doi.org/10.1529/biophysj.106.088963.
[38] M.E. Taylor, K. Drickamer, A. Imberty, Y. van Kooyk, R.L. Schnaar, M.E. Etzler, A. Varki, Discovery and classification of glycan-binding proteins, in: A. Varki, R. D. Cummings, J.D. Esko (Eds.), Essentials of Glycobiology [internet], fourth ed, Cold Spring Harbor Laboratory Press, New York, 2022, https://doi.org/10.1101/glycobiology.4e.28.